Supporting Information

Gordon et al. 10.1073/pnas.1202529109

SI Methods

Cardiovascular Testing Details. Fasting carotid-femoral pulse wave velocity (PWV_{cf}) was determined by measuring the propagation time of the pressure pulse from the carotid to femoral arteries (1). Propagation time (Δtcf) was calculated by measuring the time lag between the R-wave of the simultaneous ECG and the arrival of the arterial pulse at both the carotid (Δtc) and femoral (Δtf) arteries. The distance between the carotid and femoral arteries (lcf) was measured and recorded. PWV_{cf} was calculated using the formula PWV_{cf} = lcf/Δtcf.

Fasting diagnostic carotid artery ultrasonography was performed using established protocols (2) in a laboratory accredited by the Intersocietal Commission for the Accreditation of Vascular Laboratories. A Philips iU22 μLtrasound machine equipped with an L17–5 MHz broadband linear-array transducer was used.

Carotid stenoses were graded using velocity ratios, and pulsed-wave Doppler was performed with appropriate angle correction. Mean distal internal carotid artery velocity was calculated using a formula that adds one-third of the peak systolic velocity plus two-thirds of the end diastolic velocity, as previously described (3). Gray map 5 was used on all studies after adjusting overall gain so that intraluminal blood appeared black. Digital gain compensation was kept perpendicular.

Distal common carotid artery far-wall intima-media thickness was measured from the intima–lumen border to the media–adventitia border over a 2-cm segment according to a standard protocol (1) using edge-detection software (Medical Imaging Applications) (4).

Quadriceps Muscle Dynamometry. Quadriceps muscle strength was evaluated bilaterally using a standard method (5). The patient was positioned sitting with hip and knee flexed to 90° and with the back unsupported. Knee position was maintained to achieve an isometric contraction. Use of hands on a mat for support was permitted. A hand-held dynamometer (Model 01163; Lafayette Instrument Company) was placed on the distal anterior tibia just proximal to the ankle joint. A 3-s maximal isometric contraction was performed followed by a brief rest. Three repetitions were performed on each leg.

Lonafarnib Pharmacokinetic Analysis. Plasma concentrations of lonafarnib were determined at 115 mg/m^2 and 150 mg/m^2 at 0, 1, 2, 4, 6, and 8 h postdose by HPLC/ion chromatography (IC) tandem mass spectrometry (6). Lonafarnib pharmacokinetics (PK) were determined using noncompartmental analyses. The lower limit of quantitation for lonafarnib was 5 ng/mL with a linear standard curve over a concentration range of 5–2,500 ng/mL. The coefficient of variation and accuracy (% bias) were less than 11% and less than 10%, respectively. Individual plasma lonafarnib concentrations were used for PK analysis using model-independent methods (7). The area under the plasma-concentration time curve from time 0 to 12 h after dose [AUC(0–12)] was calculated using the linear trapezoidal method, where concentration at 0 h also was used as an estimate of plasma concentration at 12 h for each concentration–time profile (steady state achieved at 4 and 8 mo). The apparent total-body clearance at steady state was calculated by dividing the dose by AUC(0–12). Interpatient variability of the PK parameters was expressed as percent coefficient of variation. Plasma concentration values of patients who had multiple-cycle PK samples were modeled via a mixed-effects approach in an effort to explore dose and cycle effects.

Pharmacodynamics. HDJ-2 farnesylation status as a surrogate marker of lonafarnib activity was assayed in lysates from peripheral blood mononuclear cells pretherapy, at 52 wk on lonafarnib, and at end of therapy. Western blotting for HDJ-2 gel mobility shifts was performed as previously reported (8). Western blots were quantified using a Molecular Imager Gel Dock XR densitometer (Bio-Rad). Data were analyzed using Quantity One software (Bio-Rad). Samples with enough protein were run in duplicate (n = 40 of 92 samples analyzed), with close agreement between samples. Inhibition was defined as >10% of HDJ-2 in the unfarnesylated form.

SI Results

Confidence Interval Comparisons.

End point	No. patients	Point estimate (%)	90% exact binomial confidence interval (CI, %)	95% exact binomial CI (%)
≥50% Increase in rate of weight gain	9/25	36	20–54	18–58
≥3% Increase in areal bone mineral density at at least one site	19/25	76	58–89	55–91
Any decrease in bone mineral density	10/25	40	24–58	21–61
Low frequency sensorineural hearing improvement ≥ 10 dB	8/18	44	24–66	22–69

Frequency of ECG Abnormalities. Twelve-lead ECG was performed at 4-mo intervals. Fourteen of 26 patients (54%) had no abnormality identified at any time during the course of the study. At baseline, 8 of 26 patients (31%) had ECG abnormalities, compared with 4 of 25 patients (16%) at end of therapy; major ECG abnormalities on 12-lead ECG did not change significantly during the course of the study.

ECG changes consistent with left ventricular hypertrophy (LVH) with or without LV strain pattern was seen in 3 of 26 patients (12%) with a mean age of 11.9 y; borderline LVH was identified at entry or transiently during the study in four additional patients (15%). Atrial enlargement was noted in one patient with history of supraventricular tachycardia.

Isolated nonspecific ST-T wave changes were identified transiently in four patients and consistently in one patient without other abnormalities. Prolonged QT intervals (QTc > 0.44 s) were observed only transiently in 4 of 26 patients (15%), although none had QTc >0.45 s or demonstrated persistent QTc prolongation. Two patients had prior history of supraventricular tachycardia before entry, and none had uncontrolled rhythm disturbance identified during the course of study.

Significant left ventricular hypertrophy tended to be identified in older patients compared with those patients with normal ECGs or those with isolated ST-T wave changes (11.9 y vs. 6.7 y, respectively). Two of three patients with LVH had been prescribed antihypertensive medication before study entry.

Audiology. We found pretherapy conductive hearing loss in 21 of 23 children at low frequencies and in 7 of 23 children at high frequencies. At end of therapy, median hearing thresholds were significantly different for high-frequency conductive hearing in

the poorer-hearing ear ($P = 0.01$) but not in the better-hearing ear; no change was detected in low-frequency hearing in the poorer- or better-hearing ears. From a clinical perspective, no ear changed by ≥10 dB.

Pharmacodynamics. As shown in Table S6, in some patients (both responders and nonresponders), accumulation of unfarnesylated HDJ-2 was observed at only one of the two on-treatment time points. The reason for this intrapatient variability is not known. Positive controls [cultured cells treated in vitro with a farnesyltransferase inhibitor (FTI)] were included in all experiments and consistently demonstrated appropriate shifts. Variability between time points also was observed in some patient samples from a prior study of lonafarnib in cancer (see below) (9). In the study reported by Feldman et al. (9), 59 patients had evaluable HDJ-2 blots at two on-treatment time points as well as at baseline. Of these patients, 17 (29%) showed no shift in HDJ-2 at either time point, 31 (53%) showed shifts of comparable magnitude at both on-drug time points, and 11 (19%) showed shifts at only one of the two on-treatment time points evaluated (eight had shifts at cycle 1 day 15 only, and three had shifts at cycle 2 day 1 only). Although the percentages and time points for longitudinal sampling are different in the two studies, both show that the extent of inhibition of HDJ-2 farnesylation varied at different on-treatment time points.

Additional Acknowledgments. Most importantly, we are grateful to the children with progeria and their families, and to the children who participated as control subjects, for participation in this study. We thank the Family Inn (Cambridge, MA) and Devon Nicole House (Boston, MA) for housing families; Susan Campbell, MS, Nancy Wolff-Jenssen, and Nancy Grossman for medical records coordination; Kyra Johnson, Kelly Littlefield, Kiera McKendrick, Angela Kraybill, and William Fletcher for coordinator services; Ethan Bickford for photographic assistance; James Miller, CPO and National Orthotics and Prosthetics Company for podiatric assistance; administrative, nursing, and processing staff at the CHB Clinical and Translational Study Unit; David Bowling and Rocco Anzaldi, RPh for pharmacy assistance; Nicole Wake for echocardiography assistance; Marie Migliaccio for graphic art; Merck Research Labs/Schering-Plough Research Institute for providing lonafarnib, PK and PD studies; Susan Arbuck, MD, Emily Frank, MS, David Harris, PhD, Bhavna Kantesaria, MS, Paul Kirschmeier, PhD, Antoinette Lee, and Yali Zhu, MS for assistance with lonafarnib; Stephen Young, MD, Loren Fong, PhD, and Marsha Moses, PhD for biomarker evaluation; and Elizabeth Nabel, MD, for review of the manuscript.

1. O'Rourke MF, Staessen JA, Vlachopoulos C, Duprez D, Plante GE (2002) Clinical applications of arterial stiffness; definitions and reference values. *Am J Hypertens* 15: 426–444.
2. Gerhard-Herman M, et al.; American Society of Echocardiography; Society of Vascular Medicine and Biology(2006) Guidelines for noninvasive vascular laboratory testing: A report from the American Society of Echocardiography and the Society of Vascular Medicine and Biology. *J Am Soc Echocardiogr* 19:955–972.
3. Pawlak MA, et al. (2009) Sickle cell disease: Ratio of blood flow velocity of intracranial to extracranial cerebral arteries—initial experience. *Radiology* 251:525–534.
4. Roman MJ, et al.; American Society of Echocardiography; Society of Vascular Medicine and Biology(2006) Clinical application of noninvasive vascular ultrasound in cardiovascular risk stratification: Report from the American Society of Echocardiography and the Society of Vascular Medicine and Biology. *J Am Soc Echocardiogr* 19:943–954.
5. Merlini L, Mazzone ES, Solari A, Morandi L (2002) Reliability of hand-held dynamometry in spinal muscular atrophy. *Muscle Nerve* 26:64–70.
6. Appels NM, van Maanen MJ, Rosing H, Schellens JH, Beijnen JH (2005) Quantitative analysis of the farnesyl transferase inhibitor lonafarnib (Sarasartrade mark, SCH66336) in human plasma using high-performance liquid chromatography coupled with tandem mass spectrometry. *Rapid Commun Mass Spectrom* 19:2187–2192.
7. Gibaldi P, Perrier D, eds (1982) *Pharmacokinetics* (Marcel Dekker, Inc, New York), pp 409–417.
8. Adjei AA, et al. (2000) A Phase I trial of the farnesyl transferase inhibitor SCH66336: Evidence for biological and clinical activity. *Cancer Res* 60:1871–1877.
9. Feldman EJ, et al. (2008) On the use of lonafarnib in myelodysplastic syndrome and chronic myelomonocytic leukemia. *Leukemia* 22:1707–1711.

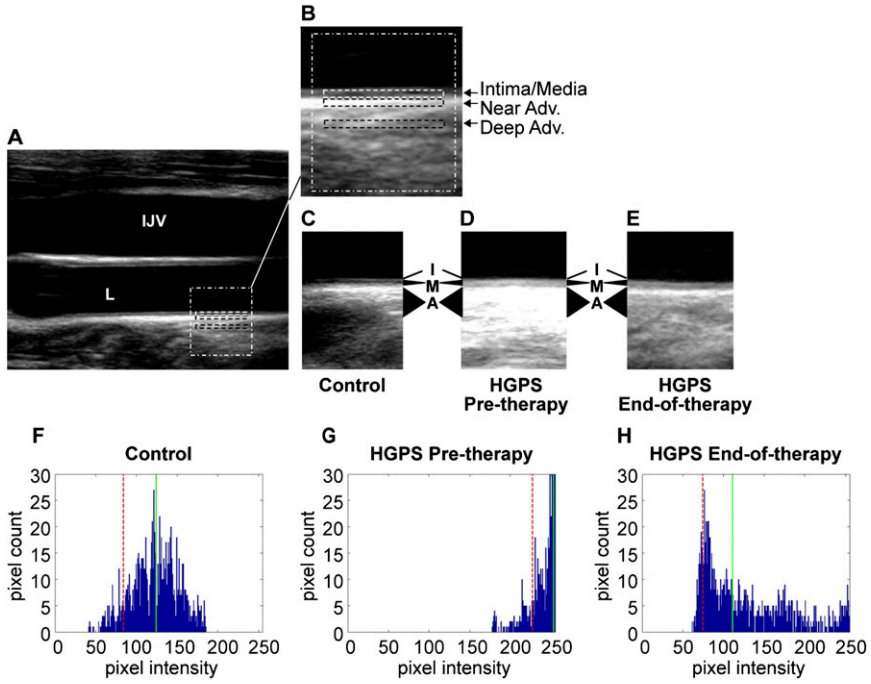

Fig. S1. Echodensity improvements with lonafarnib therapy. Carotid ultrasound images were captured for echodensity measures. (*A*) Longitudinal image of the common carotid artery in a control subject. The area of interest is indicated by large dashed rectangle. IJV, internal jugular vein; L, lumen of the common carotid artery. (*B*) Enlargement of the area of interest seen in *A* showing echodensity assessed in prespecified areas indicated by the dashed boxes in the far wall of the distal common carotid artery. The white dashed box indicates the intima-media area, and black dashed boxes indicate near-adventitia (Near Adv.) and deep-adventitia (Deep Adv.) areas measured. (*C–D*) Posterior common carotid artery wall in a control subject demonstrating normal echodensity of the intima (I), media (M), and adventitia (A) (*C*), compared with a patient with Hutchinson–Gilford progeria syndrome (HGPS) displaying increased echodensity pretherapy (*D*) and the same patient displaying normal-looking echodensity at end of therapy (*E*). (*F–H*) Histogram plots for patients shown in *C–E*. Pixel intensity (*x* axis) vs. pixel count (*y* axis) was derived from the near adventitia area of measurement. The solid green vertical line represents the 50th percentile, and the dashed red vertical line represents the 10th percentile for each plot. Note that the HGPS histogram at end of therapy is comparable to the control histogram.

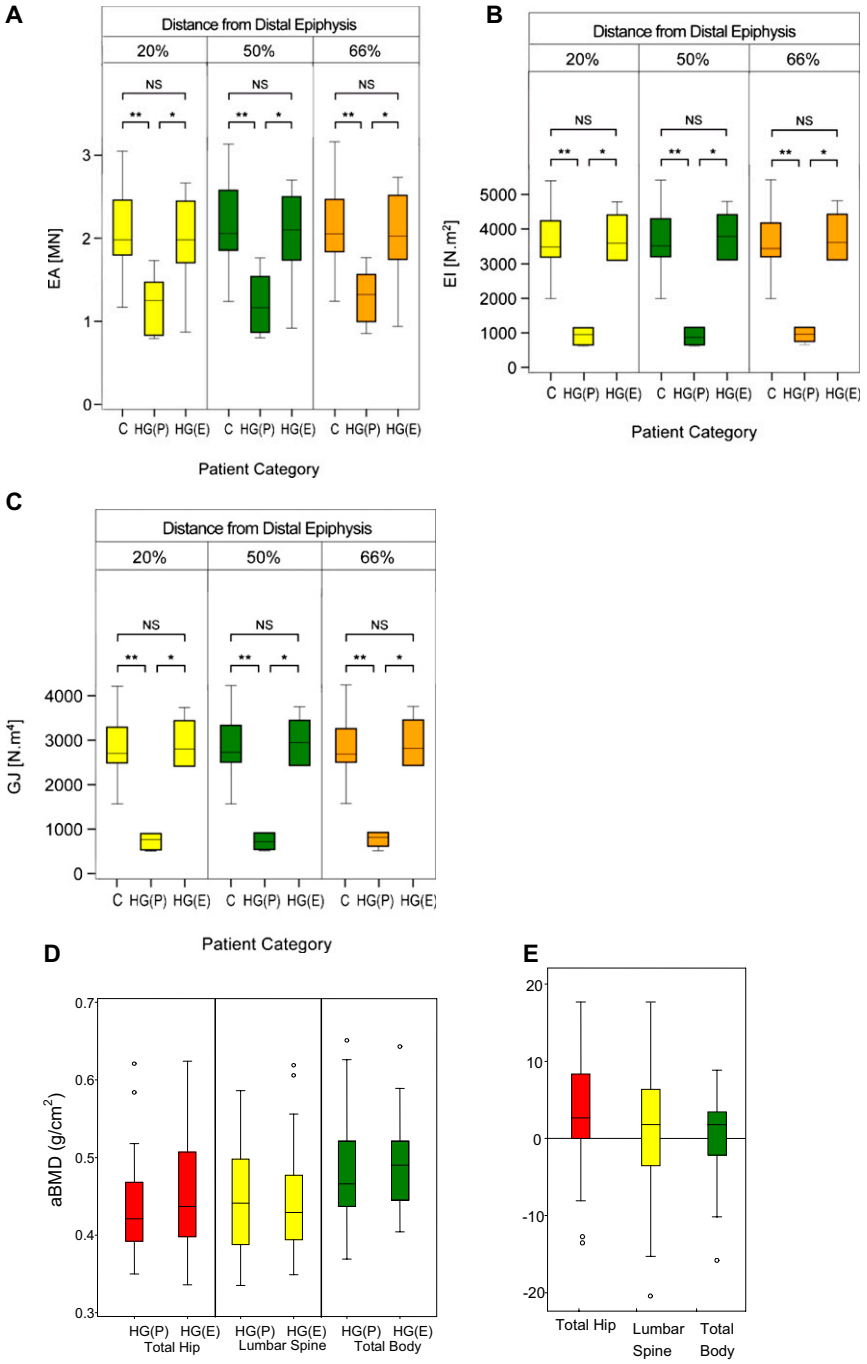

Fig. S2. Lonafarnib normalized skeletal rigidity in HGPS. Shown are means and SDs for (*A*) cross-sectional axial (EA), (*B*) bending (EI), and (*C*) torsional (GJ) rigidities at indicated radial sites in the control group (C), and in HGPS patients pretherapy [HG(P)] and at end of therapy [HG(E)]. The top and bottom box edges indicate the 75th and 25th interquartile ranges (IQR), respectively. Horizontal lines within boxes represent medians. Lower and upper whiskers represent Q1 − 1.5 × IQR and Q3 + 1.5 × IQR. *P* values for EI, EA, and GJ at all four radial sites were as follows for the control group and the HGPS group that received peripheral quantitative CT evaluation at both pretherapy and end of therapy: We detected significant abnormality between the control group and the HGPS pretherapy group (**$P < 0.0001$). We detected statistically significant improvements in abnormality in the HGPS end-of-therapy group as compared with the HGPS pretherapy group (*P 0.007–0.03). There were no statistically significant differences between the control group and the HGPS end-of-therapy group (P = 0.42–0.99, NS). For the 20, 50, and 66% radial sites, n = 58, 58, and 55, respectively, in the control groups, and n = 11, 10, and 9, respectively, in the HGPS groups. (*D* and *E*) Areal bone mineral density (aBMD) was obtained with dual X-ray absorptiometry for the HGPS patient cohort (n = 25). Means and SDs for indicated sites are shown. The top and bottom box edges represent the 75th and 25th IQRs, respectively. Horizontal lines within boxes represent medians. Lower and upper whiskers represent Q1 − 1.5 × IQR and Q3 + 1.5 × IQR, respectively. Outliers are shown as hollow circles. (*D*) aBMD for the HGPS cohort pretherapy [HG (P)] and at end of therapy [HG(E)]. (*E*) Percent change (end of therapy vs. pretreatment). P = 0.03 (hip); P = 0.33 (lumbar spine); and P = 0.15 (total body).

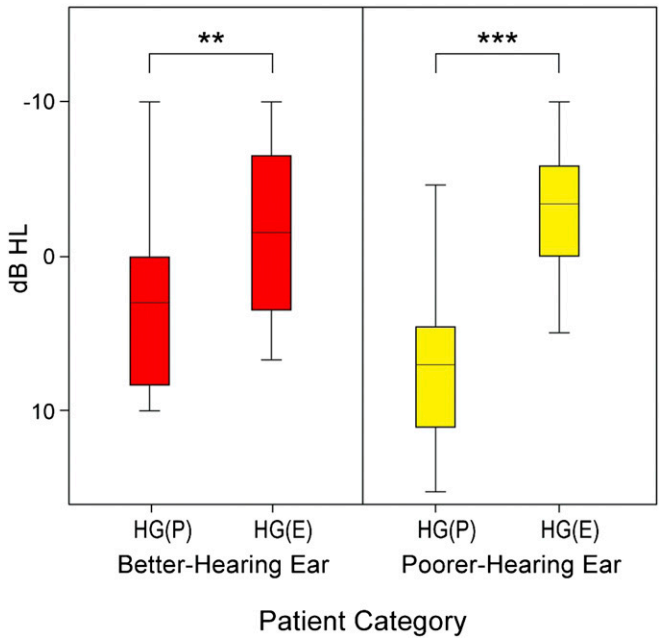

Fig. S3. Low-frequency sensorineural improvements with lonafarnib therapy. Box plots of low-frequency sensorineural hearing in the HGPS better-hearing ear (yellow) and poorer-hearing ear (red) in pretherapy [HG(P)] and end-of-therapy [HG(E)] groups. Top and bottom box edges indicate IQR 75th and 25th percentiles, respectively. Horizontal lines within boxes represent medians. Lower and upper whiskers represent Q1 − 1.5 × IQR and Q3 + 1.5 × IQR. $^{**}P = 0.008$; $^{***}P = 0.0002$.

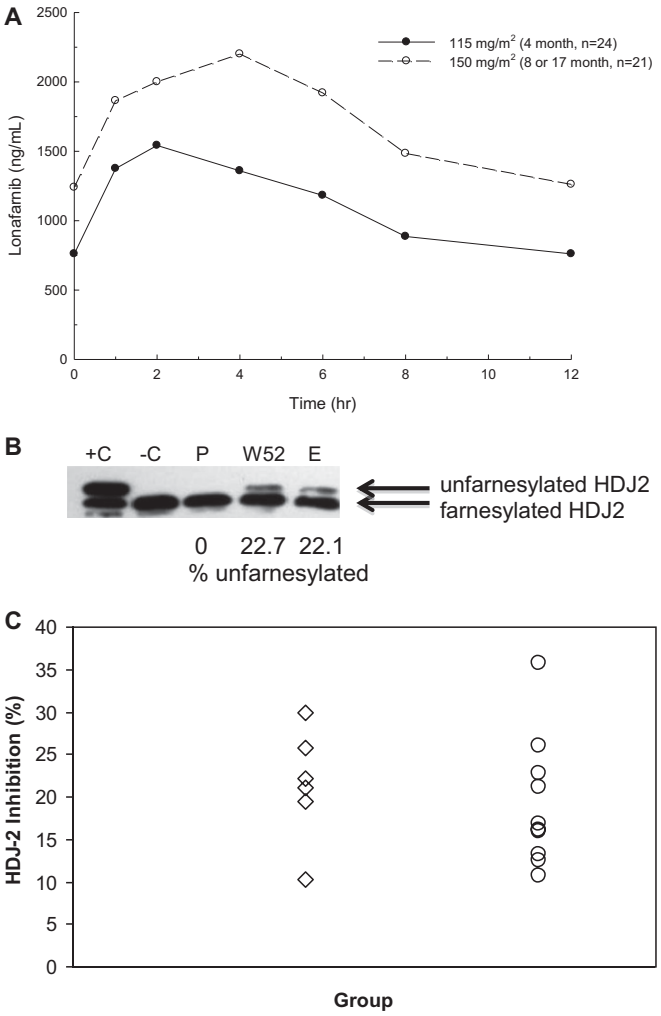

Fig. S4. Lonafarnib pharmacokinetics. (*A*) Mean plasma lonafarnib concentration (*y* axis) over a 12-h dosing period (*x* axis) at doses of 115 mg/m^2 (solid lines with filled circles; $n = 24$) and 150 mg/m^2 (dashed lines with open circles; $n = 21$). (*B*) Sample Western blot showing a single subject's HDJ-2 farnesylation status at pretreatment (P), midtrial at 52 wk on therapy (W52), and at end of therapy (E). C, control (A549 human lung adenocarcinoma cell culture ± FTI treatment). (*C*) Assessment showed those subjects with shifts in HDJ-2 from the farnesylated to the unfarnesylated form were similar, regardless of whether the subjects exhibited improvement in rate of weight gain (open diamonds; $n = 6$ of 9) or lack of improvement in rate of weight change (open circles; $n = 9$ of 16).

Table S1. Toxicities possibly related to lonafarnib

Toxicity	Grade	No. patients exhibiting toxicity during entire trial period* (n = 26)	Number of patients exhibiting toxicity during time period specified (months on treatment)					
			0–4	4–8	8–12	12–16	12–16	20–end
Gastrointestinal								
Diarrhea	1	21	21	18	19	16	14	17
	2	2	1	0	0	1	1	0
	3	3	0	0	0	1	1	1
Vomiting	1	13	13	13	11	9	5	4
	2	4	3	0	1	0	1	0
	3	2	1	0	0	0	1	0
Dehydration	3	1	0	0	0	1	0	0
Constipation	1	7	7	2	0	0	0	0
	2	1	1	0	0	0	0	0
Dyspepsia	1	1	0	0	0	1	0	0
Constitutional								
Fatigue	1	14	10	3	3	5	5	4
	2	2	1	0	0	1	1	1
Nausea	1	13	13	6	2	2	2	2
	2	1	0	0	0	1	0	0
Anorexia	1	10	9	4	5	5	4	5
	2	2	0	0	1	0	1	0
Fever	1	9	4	2	5	2	0	1
	2	2	0	0	0	1	1	0
	4	1	0	0	0	0	1	0
Organ function								
Elevated AST	1	11	4	3	2	3	2	4
	3	1	1	0	0	0	0	0
Elevated ALT	1	8	5	2	2	2	2	2
	2	1	1	1	0	0	0	0
	3	1	1	0	0	0	0	0
Elevated alkaline phosphatase	1	2	1	1	0	1	0	0
	2	2	0	0	2	0	0	0
Low Absolute Leukocyte Count	1	3	0	1	0	2	1	0
	2	2	0	0	1	2	0	0
Low white blood cell count	1	10	4	3	5	5	5	1
Low absolute neutrophil count	1	14	7	6	10	5	6	5
	2	3	1	1	0	0	2	0
Low hemoglobin	1	9	9	3	5	5	6	2
	2	2	0	2	2	0	0	1
Metabolic								
Hypermagnesemia	1	7	5	3	2	1	1	1
Hyperkalemia	1	3	2	2	1	0	1	1
Hypokalemia	1	2	1	0	0	0	1	0
	3	4	0	1	0	2	1	0
Hyponatremia	1	11	3	5	3	2	2	5
Hypocalcemia	1	1	0	0	0	0	0	1
	2	1	0	0	0	0	0	1
Hypercalcemia	1	6	3	2	1	2	0	1
Depressed serum bicarbonate	1	10	5	6	1	3	4	4
Hypoglycemia	1	2	2	1	1	1	1	1
	2	1	1	0	0	0	0	0
	3	1	0	0	0	1	0	0
Hyperglycemia	1	4	1	2	0	0	1	1
	2	2	0	0	0	0	1	1
Other								
Granuloma	1	1	1	1	1	1	1	1
Perineal edema	1	1	0	1	1	0	0	0
Raynaud's phenomenon	2	1	0	0	0	1	0	0

*Per patient count is once for that patient's highest toxicity grade.

Table S2. Factors contributing to rate of weight gain

Factor	Weight gain end point: Achieved (n = 9)* Median	Achieved (n = 9)* Range	Not achieved (n = 16)* Median	Not achieved (n = 16)* Range	Wilcoxon rank-sum P value
Body composition					
Total lean tissue mass (g)					
Pretreatment	7,334.5	5,632.1–15,036.8	8,815.9	5,531.4–13,865.8	
Posttreatment	8,269.8	6,665.7–17,022.5	9,405.9	5,333.0–14,276.2	
Fold change	1.10	1.07–1.18	1.05	0.89–1.14	0.005
Total aBMD(g/cm^2)					
Pretreatment	0.437	0.413–0.601	0.491	0.369–0.651	
Posttreatment	0.449	0.420–0.643	0.500	0.404–0.589	
Fold change	1.04	0.96–1.08	1.01	0.85–1.09	0.04
Total fat mass (g)					
Pretreatment	1,757.0	11,86.6–2,109.1	1,482.9	11,58.7–4,059.8	
Posttreatment	1,675.4	1,250.8–2,669.9	1,613.3	12,09.0–2,379.7	
Fold change	0.93	0.69–1.76	1.06	0.54 –1.33	0.78
Total % body fat					
Pretreatment	17.0	11.0–24.0	14.3	9.3– 31.6	
Posttreatment	15.5	12.8–24.1	15.1	10.0– 20.8	
Fold change	0.84	0.69–1.48	1.02	0.57–1.24	0.50
Energy balance					
Total energy intake (kcal/d)					
Pretreatment	1,089	859–1,601	1236	680–1,625	
Posttreatment	1,062	834–2,246	1271	834– 2,020	
Fold change	1.00	0.59–1.48	0.99	0.69– 2.83	0.75
Energy intake as % RDA					
Pretreatment	130	96–195	165	96–,279	
Posttreatment	136	95–209	176	141– 272	
Fold change	1.03	0.551–.61	1.15	0.79– 2.67	0.48
MREE(kcal/d)					
Pretreatment	641	499–857	589	241– 889	
Posttreatment	715	567–898	677	379–931	
Fold change	1.13	0.87–1.29	1.12	0.73–1.98	0.82
Quadriceps muscle strength					
Left quadriceps (kg)					
Pretreatment	5.4	3.0–11.7	5.6	2.2–11.4	
Posttreatment	5.6	4.01–0.8	5.1	3.0–10.6	0.93
Fold change	1.1	0.7–1.4	1.0	0.8–1.6	
Right quadriceps (kg)					
Pretreatment	6.0	3.4–9.2	5.6	3.0–12.6	
Posttreatment	5.8	3.9–13.0	5.7	3.0–11.7	
Fold change	1.1	0.8–1.7	1.0	0.7–1.2	0.26

aBMD, areal bone mineral density; MREE, measured resting energy expenditure; RDA, recommended dietary allowance.
*One patient in the achieved group and four patients in the not-achieved group received recombinant growth hormone therapy.

Table S3. Effect of lonafarnib on carotid artery density by ultrasound

Site	Percentile	Median density in pixels (range): Control (n = 55)	HG(P) (n = 22)	HG(E) (n = 22)	P value: Control vs. HG(P)*	HG(P) vs. HG(E)†	Control vs. HG(E)*
Intima media	10	52.0 (8.0–107.0)	61.0 (8.0–174.0)	41.0 (0.0–93.0)	0.02	0.002	0.68
Adventitia luminal near wall	10	112.0 (49.0–193.0)	159.0 (33.0–246.0)	103.0 (40.0–215.0)	0.002	0.005	0.47
Adventitia deep near wall	10	132.0 (5-226.0)	102.0 (10.0–228.0)	88.0 (0.0–169.0)	0.06	0.04	<0.0001

HG(E) HGPS, end of therapy; HG(P), HGPS pretherapy.
*Based on Wilcoxon rank-sum test.
†Wilcoxon signed-rank test based on distributions of fold-change (post/pre) calculated for each patient.

Table S4. Clinically significant changes in areal BMD (n = 25)

Site	No. patients with >3% increase	No. patients with >3% decrease	No. patients with no significant change*
Total body	11	4	10
Lumbar spine	11	7	7
Hip	11	4	10

*Change between −3% and +3%.

Table S5. Lonafarnib pharmacokinetics

Mean (CV,%) PK parameters for lonafarnib

Dose (mg/m^2)	115 (n = 24)	150 (n = 21)
Cmax (μg/mL)	1.77 (60)	2.64 (41)
Median Tmax (h) (range)	2.0 (0–6)	4.0 (0–6)
AUC(0–12 h)(μg·h^{-1}·mL^{-1})	13.2 (62)	20.6 (36)

CV, Coefficient of variation; Cmax, maximum concentration; Tmax, time to maximum concentration.

Table S6. Lonafarnib pharmacodynamics: Patients with unfarnesylated HDJ-2 detected at week 52 and/or end of study (n = 25)

Detected at week 52 on therapy	Detected at end of study	No. (%) with unfarnesylated HDJ-2
No	No	12 (48)
Yes	No	6 (24)
No	Yes	3 (12)
Yes	Yes	4 (16)